Resilience of Majorana fermions in the face of disorder

Alireza Habibi,[1] S. A. Jafari,[1,*] and S. Rouhani[1,2]
[1]*Department of Physics, Sharif University of Technology, Tehran 11155-9161, Iran*
[2]*Institute for Research in Fundamental Sciences (IPM), Tehran 19395-5531, Iran*

(Received 13 April 2018; revised manuscript received 7 July 2018; published 26 July 2018)

We elucidate the reduction of the winding number caused by the on-site disorder in a next-nearest-neighbor XY model. When disorder becomes strong enough, Majorana edge modes become critically extended, beyond which they collapse into Anderson localized (AL) states in the bulk, resulting in a topological Anderson insulating state. We identify a resilience threshold W_t for every pair of Majorana fermions (MFs). In response to increasing disorder, every pair of MFs collapse into AL states in the bulk beyond their resilience threshold. For very strong disorder, all Majorana fermions collapse, and a topologically trivial state is obtained. We show that the threshold values are related to the localization length of Majorana fermions, which can be efficiently calculated by an appropriate modification of the transfer-matrix method. At the topological transition point, the localization length of the zero modes diverges, and the system becomes scale invariant. The number of peaks in the localization length as a function of disorder strength determines the number of zero modes in the clean state before disorder is introduced. This finding elevates the transfer-matrix method to the level of a tool for the determination of the topological index of both clean and disordered systems.

DOI: 10.1103/PhysRevB.98.035142

I. INTRODUCTION

Generically, topology protects the system against weak disorder. However, when disorder can close the gap, it can change topological properties [1]. Therefore when disorder becomes strong, it can affect the topology and can lead to a quantum phase transition to the so-called topological Anderson insulating (TAI) state [2]. The interplay between disorder and topology has been studied in the past [2]. The change in Hall conductance as a function of disorder in a two-dimensional square lattice was numerically investigated in Ref. [3]. In the presence of a disorder that breaks the symmetries but preserves them in ensemble averages, the system is still strictly characterized by topological numbers [4], although they may be different numbers compared to the clean system. In the vicinity of the topological Anderson transition, the Chern number in finite-size two-dimensional systems smoothly changes across the two topological phases. For an infinite system, the change becomes a sharp step function [5,6]. The Kitaev chain with a quasiperiodic potential with a Fibonacci sequence shows an interplay of fractal structure and topology for Fibonacci potentials in the topological phase diagram [7]. In a two-dimensional bipartite lattice, the topological number survives up to a much stronger disorder (one order of magnitude higher) if only one of the sub-lattices is disordered and the final state in the strongly disordered system is in the metallic phase [8].

Quadratic Hamiltonians have been classified by Altland and Zirnbauer into ten classes [9] based on symmetry classes of random matrices [10]. In every space dimension, five of the ten symmetry classes of the Altland-Zirnbauer classification have nontrivial topology [10]. In one-dimensional systems, these five topologically nontrivial classes are D and DIII, which are classified with a Z_2 index, and three chiral classes, AIII, BDI, and CII, which have Z classification. Recently, a generalization of XY spin chain [11] was proposed which after fermionization corresponds to the BDI class of topological superconductors [12]. This model can be classified with an integer winding number (WN). This extension called nXY in Ref. [12] allows for engineering a Hamiltonian with any desired WN. Therefore it provides a playground to study systems with larger WNs and hence a larger number of Majorana fermions. A similar extension of the Ising model in the transverse field Hamiltonian exists [13]. In this work, we study the effect of disorder on the topological properties of the second-neighbor generalization of the XY model (2XY model) [12]:

$$H_{2\mathrm{XY}} = \sum_j (J_1+\lambda_1)\sigma_j^x\sigma_{j+1}^x + (J_1-\lambda_1)\sigma_j^y\sigma_{j+1}^y + (J_2+\lambda_2)\sigma_j^x\sigma_{j+1}^z\sigma_{j+2}^x + (J_2-\lambda_2)\sigma_j^y\sigma_{j+1}^z\sigma_{j+2}^y, \tag{1}$$

which after Jordan-Wigner (JW) fermionization becomes

$$H_{2\mathrm{XY}}^{\mathrm{JW}} = 2\sum_{s=1,2}\sum_j J_s c_j^\dagger c_{j+s} + \lambda_s c_j^\dagger c_{j+s}^\dagger + \mathrm{H.c.} \tag{2}$$

This Hamiltonian allows for WNs up to 2. In this class, any short-range correlated disorder is enough to cause Anderson localization of all quasiparticles [14]. For open boundary conditions, there can exist some symmetry-protected (Majorana) zero modes which are localized on the boundary [15]. Strong disorder at transition points will change localized topological states to Anderson localized states. This transition was dubbed the topological Anderson transition [2]. The special case for $J_1 = \lambda_1$ and $J_2 = \lambda_2$ was studied in Refs. [16,17].

*akbar.jafari@gmail.com

II. MODEL HAMILTONIAN

The Hamiltonian we study is given by

$$H = H_{2\mathrm{XY}} + H_{\mathrm{dis}}, \tag{3}$$

where the translation-invariant part $H_{2\mathrm{XY}}$ of the model is given by Eq. (2). The random-field term H_{dis} has the following form:

$$H_{\mathrm{dis}} = \sum_j (\varepsilon_j + \mu)\sigma_j^z, \tag{4}$$

where ε_j is uniformly distributed in the interval $[-W/2, W/2]$.

The clean system can be solved with JW transformation [12]:

$$\sigma_j^z = 2c_j^\dagger c_j - 1, \quad \sigma_j^x = e^{i\phi_j}(c_j^\dagger + c_j), \quad \sigma_j^x = ie^{i\phi_j}(c_j^\dagger - c_j), \tag{5}$$

where $\phi_j = \pi \sum_{l<j} c_l^\dagger c_l$ is the phase string. With this transformation the entire Hamiltonian becomes

$$H = 2\sum_{s=1,r}\sum_j J_s c_j^\dagger c_{j+s} + \lambda_s c_j^\dagger c_{j+s}^\dagger + \mathrm{H.c.} + 2\sum_j (\varepsilon_j + \mu)\left(c_j^\dagger c_j - \frac{1}{2}\right). \tag{6}$$

This makes it clear that μ is the chemical potential of the JW fermions. This model is an extension of the Kitaev chain model of a p-wave superconductor where next-nearest-neighbor hoppings and pairings along with on-site disorder have been added.

In terms of Nambu spinors $\psi^\dagger = (c^\dagger \quad c)$ we have

$$H = \psi^\dagger \begin{pmatrix} \tilde{H}_0 & \tilde{\Delta} \\ \tilde{\Delta}^\dagger & -\tilde{H}_0 \end{pmatrix} \psi \equiv \psi^\dagger \tilde{H} \psi, \tag{7}$$

or, equivalently, introducing Pauli matrices $\vec{\tau}$ for the Nambu space, the matrix representation of the Hamiltonian becomes

$$\tilde{H} = \tilde{H}_0 \otimes \tau_z + i\tilde{\Delta} \otimes \tau_y, \tag{8}$$

where $\tilde{H}_0$ and $\tilde{\Delta}$ are the following matrices:

$$\tilde{H}_0 = \sum_{s=1,r}\sum_j (J_s |j\rangle\langle j+s| + \mathrm{H.c.}) + \sum_j (\varepsilon_j + \mu)(|j\rangle\langle j|), \tag{9}$$

$$\tilde{\Delta} = \sum_{s=1,r}\sum_j (\lambda_s |j\rangle_e \langle j+s|_h - \lambda_s |j+s\rangle_e \langle j|_h). \tag{10}$$

Note that since the matrix $\tilde{\Delta}$ is off diagonal in the Nambu space, the projection operators used in the definition of $\tilde{\Delta}$ are indeed of the $|\,\rangle_e\langle\,|_h$ form. Apparently, we have $\Delta^\dagger = -\Delta$. The $\tilde{H}_0$ part is diagonal in the Nambu space, and hence an e or h subscript is not necessary. The operator for the particle-hole symmetry can be defined as $S = \mathbb{1} \otimes \tau_x$, where $\mathbb{1}$ acts on the space of site indices $j = 1, \ldots, N$ and τ_x acts on the Nambu space, which simply replaces c and $c^\dagger$ and can be seen to affect the Hamiltonian as

$$S^{-1} H S = -H. \tag{11}$$

This model belongs to the BDI class of topological superconductors [12]. This is exactly solvable, and in Sec. III, we obtain a closed-form formula for the winding number of the clean system which varies between -2 and $+2$.

III. EXACT WN FOR CLEAN 2XY MODEL

Let us add an arbitrary chemical potential to Eq. (2) which gives an extension of the Kitaev model of topological superconductor [15] as follows:

$$H = 2\sum_j \sum_{s=1,2} J_s c_j^\dagger c_{j+s} + \lambda_s c_j^\dagger c_{j+s}^\dagger + \mathrm{H.c.} + 2\sum_j \mu\left(c_j^\dagger c_j - \frac{1}{2}\right). \tag{12}$$

This Hamiltonian can be rewritten in terms of Majorana fermions $a_i = c_i^\dagger + c_i$ and $b_i = i(c_i^\dagger - c_i)$, which obey anticommutation rules

$$\{a_i, a_j\} = \{b_i, b_j\} = 2\delta_{i,j}, \quad \{a_i, b_j\} = 0 \tag{13}$$

and furthermore are self-adjoint, $a_i^\dagger = a_i, b_i^\dagger = b_i$. The Hamiltonian in terms of Majorana fermions becomes

$$H = i\sum_{s=1,2}\sum_j (J_s - \lambda_s) a_j b_{j+s} + (-J_s - \lambda_s) b_j a_{j+s} + \frac{\mu}{2}(a_j b_j - b_j a_j). \tag{14}$$

It can be represented in k space as

$$H = \sum_{k \in BZ} (a_k \quad b_k) \begin{pmatrix} 0 & h(k) \\ h(k)^* & 0 \end{pmatrix} \begin{pmatrix} a_{-k} \\ b_{-k} \end{pmatrix}, \tag{15}$$

where

$$\frac{h(k)}{2} = i\left(J_1 \cos k + J_2 \cos 2k + \frac{\mu}{2}\right) + (\lambda_1 \sin k + \lambda_2 \sin 2k). \tag{16}$$

This Hamiltonian is invariant under time-reversal symmetry and particle-hole symmetry and belongs to class BDI [12]. This canonical form allows us to calculate the WN as [18]

$$n_w = \frac{1}{2\pi}\mathrm{Im}\int_{-\pi}^{\pi} dk h(k)^{-1}\partial_k h(k). \tag{17}$$

For $h(k) = r_k e^{i\theta_k}$ one gets $n_w = \frac{1}{2\pi}\int_{-\pi}^{\pi} dk \partial_k \theta_k = n$, where $n \in \mathbb{Z}$ and

$$\theta_k = \arctan \frac{J_1 \cos k + J_2 \cos 2k + \frac{\mu}{2}}{\lambda_1 \sin k + \lambda_2 \sin 2k}. \tag{18}$$

Observe that θ_k is *not* continuous for k in the range $[-\pi, \pi]$. To correctly count the total phase winding, one has to exclude such singular points. Therefore we break the integration into

$$n_w = \sum_{P_i} \frac{1}{2\pi}\int_{P_i^+}^{P_{i+1}^-} dk \partial_k \theta_k = \frac{1}{2\pi}\sum_{i=0,N-1} \theta_k \Big|_{P_i^+}^{P_{i+1}^-}, \tag{19}$$

where $P_0 = -\pi$ and $P_N = \pi$ and other $P_i, i = 1, \ldots, N-1$ are singular points of Eq. (18). In the present model, we have three singular points θ_k at $P_1 = \arccos\frac{-\lambda_1}{2\lambda_2}$, $P_2 = \pi - \arccos\frac{-\lambda_1}{2\lambda_2}$, and $P_3 = 0$. Obviously, points P_1 and P_2

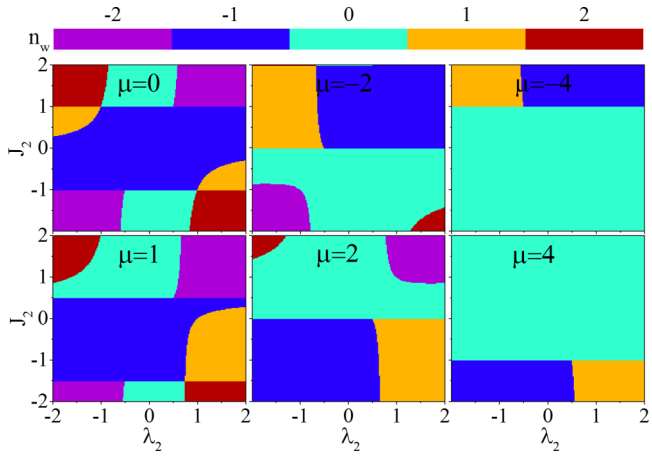

FIG. 1. Map of the WN for the clean 2XY model for various values of the chemical potential.

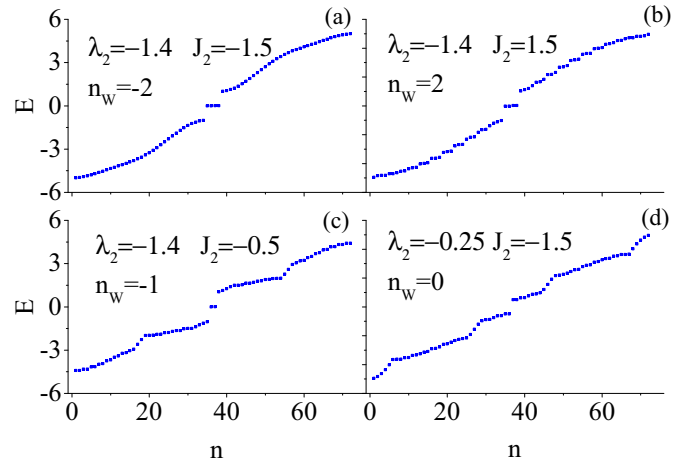

FIG. 2. Energy eigenvalues for different values of λ_2 and J_2. For the open boundary condition, we have four, two, and zero zero-energy Majorana modes for different values of λ_2 and J_2.

are present as long as $|\lambda_1| \leqslant |2\lambda_2|$. With these provisions, straightforward algebra gives

$$
\begin{aligned}
n_w = &-\frac{1}{2}\mathrm{sgn}\left[\left(-J_1+J_2+\frac{\mu}{2}\right)(-\lambda_1+2\lambda_2)\right] \\
&-\frac{1}{2}\mathrm{sgn}\left[\left(+J_1+J_2+\frac{\mu}{2}\right)(+\lambda_1+2\lambda_2)\right] \\
&-\Theta\left(1-\left|\frac{\lambda_1}{2\lambda_2}\right|\right)\mathrm{sgn}\left[-\frac{\lambda_1^2}{2\lambda_2}+2\lambda_2\left(\frac{\lambda_1^2}{2\lambda_2^2}-1\right)\right] \\
&\times \mathrm{sgn}\left[-\frac{J_1\lambda_1}{2\lambda_2}+J_2\left(\frac{\lambda_1^2}{2\lambda_2^2}-1\right)+\frac{\mu}{2}\right]. \qquad (20)
\end{aligned}
$$

Here Θ is the Heaviside function. The allowed WNs in this model are $n_w = -2, -1, 0, 1, 2$, which are plotted for various values of the chemical potential μ in Fig. 1. For zero chemical potential, the phase diagram is given by the top left panel of Fig. 1. This is in agreement with Ref. [12]. After adding the disorder term H_{dis} we will be interested in the $\mu = 0$ case, which will allow us to compare the phase diagram of the disordered system with the phase diagram of the clean system considered in Ref. [12]. Note that the units are chosen such that $J_1 = 1$. Furthermore, we fix $\lambda_1 = 1$ and let J_2 and λ_2 vary. At $\mu = 0$, one can also do exact diagonalization on a small $L = 40$ system to see the correspondence between the winding number and the number of Majorana fermion (MF) pairs. In Fig. 2 we show the number of zero-energy states and read the WN from the top left panel of Fig. 1. As can be seen, the sign of the winding number does not matter, and the number of Majorana zero modes is given by $2|n_w|$, meaning that every WN corresponds to one *pair* of MFs. The a-type MF is localized at one end, while the partner MF of the b type is localized at the other end. Sign reversal of the WN simply swaps the a and b partners across the chain [12].

IV. INDICATIONS OF RESILIENCE

As shown in Fig. 2, each WN (irrespective of its sign) corresponds to a pair of zero modes localized at two ends of the system. The sign of the WN can be changed by simply renaming a and b MFs that compose a fermion. Now let us add the on-site Anderson disorder $\sum_i \varepsilon_i c_i^\dagger c_i$, where the on-site energies are uniformly distributed in a range of width W. Unless otherwise specified, we will do most of the analysis for representative parameter values $J_2 = -1.5, \lambda_2 = -1.4$, corresponding to $n_w = -2$, where there are two pairs of MFs.

A. Spectral manifestations

In Fig. 3 we present the square of zero-energy eigenfunctions for $L = 10^3$ sites. We focus on those MFs that for small values of disorder are localized on the right edge of the system. By increasing disorder, at the first threshold value, $W_{t1} \approx 10.5$, the first pair of MFs is unpinned from the edge, while the second mode still persists and remains edge localized. Eventually, beyond a larger threshold, $W_{t2} \approx 21$, the second pair of MFs is also Anderson localized into the bulk.

To see what is happening in the Hilbert space, look at Fig. 4. Here we have plotted the density of states (DOS) for various values of the disorder. The left panel indicates that by increasing disorder, the clean superconducting gap of the spectrum is gradually filled by the level repulsion mechanism.

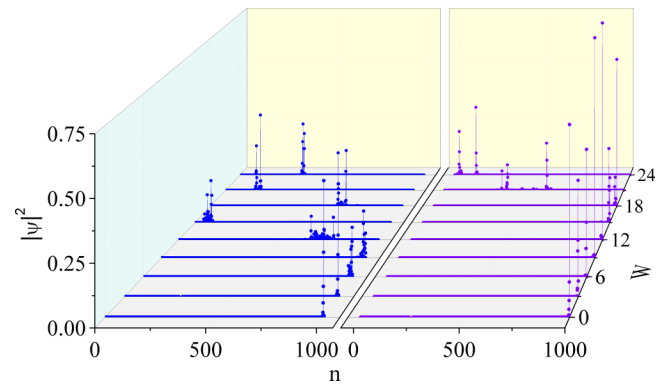

FIG. 3. Zero-energy wave functions for two types of zero modes. The first pair of MFs becomes Anderson localized (AL) upon crossing W_{t1} (left), and the second pair is AL after crossing W_{t2} (right). This calculation was done for $L = 10^3$ sites.

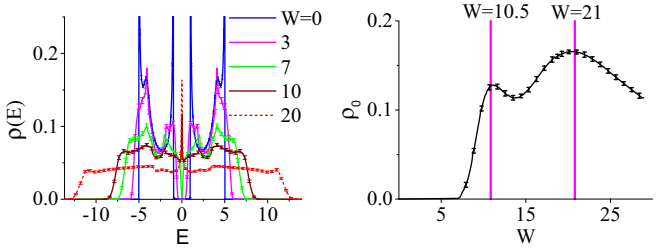

FIG. 4. Left: The DOS for the disordered system, denoted by ρ, is obtained with the kernel polynomial method (Appendix A). Due to level repulsion, when disorder increases, the gap will be filled. Right: The DOS at the middle of spectrum, $E = 0$, denoted by ρ_0, is plotted as a function of disorder strength W. The resilience threshold shows up as a maximum in the ρ_0 versus W curve.

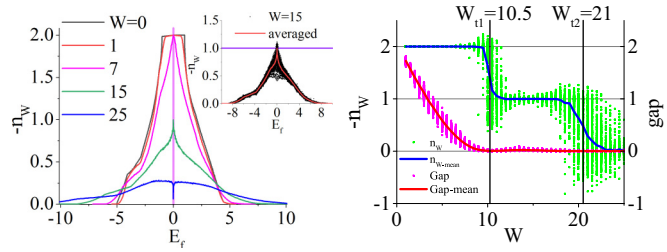

FIG. 5. Left: The WN as a function of Fermi energy E_F for various values of disorder W. Inset: Sharp pins n_w of the half-filled system averaged to integer values. Right: WN at half filling for $L = 1000$ sites (blue) and the spectral gap (red) with 100 configurations. The region between the first and second threshold is a TAI.

In the right panel, which is obtained with the kernel polynomial method [19–22], we plot the DOS ρ_0 at $E = 0$ as a function of disorder strength W. In this method (see Appendix A), we take the system size $L = 10^5$, expanding up to order $N_c = 10^3$ in Chebyshev polynomials and average over 10^2 disorder realizations. Curiously, the threshold values, W_{t1} and W_{t2} in Fig. 3, now show up as enhancements in ρ_0. This indicates that although every pair of MFs is localized at two ends of the system, the proliferation of states around $E = 0$ causes an indirect hybridization. Disorder will eventually displace them from $E = 0$. This is the DOS manifestation of the resilience threshold of MFs against the on-site disorder. Every pair of MFs is spatially pinned to the edge and energetically pinned to $E = 0$. This pinning is protected by topology, as long as the disorder is not strong enough. But strong enough disorder causes unpinning and breaks them pair by pair into the bulk and converts them to Anderson localized states.

B. Effect of disorder on WN

To understand the meaning of the two thresholds beyond which a pair of MFs is collapsed into the bulk, we need to study the change in the topological number as a function of the disorder. As we will see, at the resilience threshold, the WN of the system changes by 1. We use the method of Prodan *et al.* [18,23] to calculate the WN for disordered systems (see Appendix B). The WN of a system is obtained by summing over the occupied states. Therefore it crucially depends on the position of the Fermi level E_F that separates filled and empty single-particle states. As can be seen in the left panel of Fig. 5, when the Fermi energy crosses either the conduction or valence band, the WN will not be an integer number. But when E_F is in the middle of the spectrum, it is an integer. The inset indicates that averaging over disorder sharpens the WN. Our focus will be on the WN for $E_F = 0$, which is shown in the right panel of Fig. 5. As we increase W, there are two topological phase transitions, across which WN changes as $-2 \to -1 \to 0$. Averaging over 10^2 configurations produces smooth steplike functions. For larger systems, the steps get sharper. At the first topological phase transition at $W_{t1} \sim 10.5$, where two MFs across the ends of the system annihilate each other (see Fig. 3), the WN changes from -2 to -1. Simultaneously, the spectral gap collapses entirely. At this point the system is an Anderson insulator, but still with a nonzero WN, $n_w = -1$. It is therefore qualified to be a TAI. This TAI phase persists until a second threshold value of $W_{t2} \sim 21$, at which the remaining Majorana end modes annihilate each other by critically delocalizing over the entire system. Beyond this point, the entire system is a trivial Anderson insulator.

By repeating the above analysis for a range of values (λ_2, J_2) we can map the phase diagram of topological phases of the disordered 2XY model (Fig. 6). In a clean system [12], there are borders across which the WN changes by 2, as well as borders across with the WN changes by 1. Note that the WN changes stepwise by one unit. Thus between each two phases having WNs of n_w and $n_w \pm 2$, a nearby region with the WN $n_w \pm 1$ penetrates. Eventually, at very large values of disorder, the region with vanishing WN conquers the entire phase diagram, and the system will be a trivial Anderson localized insulator.

Although the ultimate fate of the model is to end up in the topologically trivial state, there are certain topologically trivial regions in the clean system, e.g., the region near $(\lambda_2, J_2) \approx (-1, 2)$, which acquire a *disorder-induced topology*, as can be seen in the $W = 5$ panel of Fig. 6. In the disordered system, the WN changes by 1 across all borders. The regions of $n_w = \pm 1$ inserted by disorder between $n_w = \pm 2$ and $n_w = 0$ are TAI.

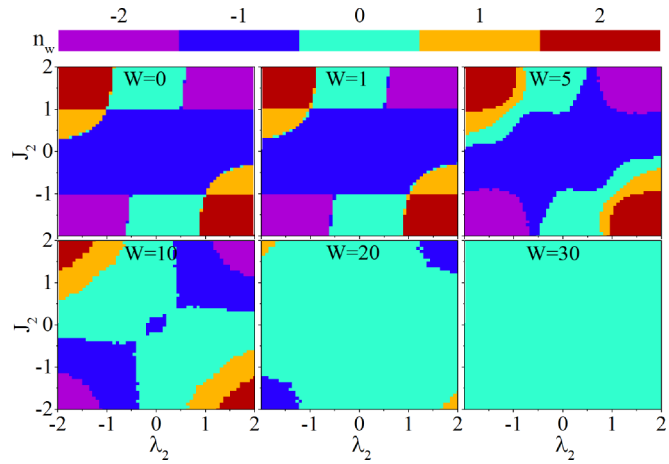

FIG. 6. Topological phases of the disordered 2XY model. The data are obtained for the system size $L = 10^3$ with an average over 100 configurations.

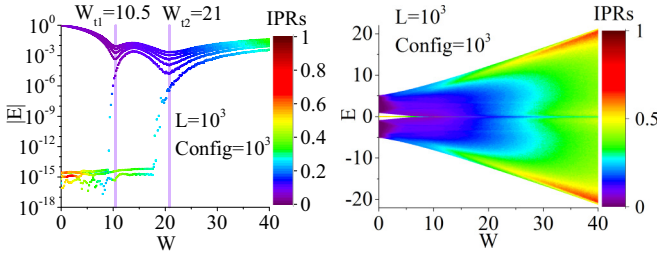

FIG. 7. Left: Tower of low-lying states as a function of disorder. The vertical axis is the absolute value of energy $|E|$. The color code indicates the IPRs. Right: Intensity map of the average IPRs for the whole spectrum as a function of disorder strength.

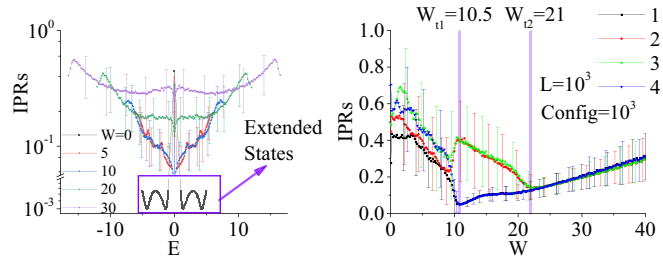

FIG. 8. Left: Constant disorder IPRs vs E. MFs at zero energy are localized even for a clean system. Right: IPRs for $E = 0$ Majorana end modes. The resilience threshold is the turning point in the IPRs.

V. RESILIENCE AND LOCALIZATION

To investigate how the resilience thresholds show up in various indicators of Anderson localization, we start by discussing inverse participation ratios (IPRs), which require exact diagonalization and are numerically very costly. After establishing the resilience threshold with this method, we shall suggest an efficient and very fast algorithm to precisely determine how disorder induces a change in topology. This will provide an alternative way of determining the topological number. This method applies equally well to clean and disordered systems. For a wave function $\psi_{i,\lambda}$ at energy eigenvalue E_λ, the IPR is defined by $P(\lambda) = \sum_i (\psi_{i,\lambda}^2)^2 / (\sum_i \psi_{i,\lambda}^2)^2$, where i denotes the lattice site. For extended states, it vanishes like $1/N$ for large N. A plane wave is an extreme example of this sort. The other extreme is a state sharply localized in one site for which $P = 1$. Therefore for more localized states, P is closer to 1, and for fully extended states, it is zero within $O(1/N)$ accuracy.

The left panel of Fig. 7 shows IPRs for low-lying parts of the tower of states as a function of disorder W. The vertical axis denotes the absolute value of energy $|E|$. As can be seen for large disorder strength, states are pushed from both positive and negative sides (due to particle-hole symmetry) towards $E = 0$ and develop a dip at two threshold values. The energy of MFs is zero within machine precision of $\sim 10^{-16}$. Near the threshold values W_{t1} and W_{t2} the MFs cannot remain pinned to $E = 0$ anymore. This unpinning is signaled in the gradual reduction of IPRs, which is, in turn, encoded into the color code. The right panel of Fig. 7 shows the intensity map of IPRs for the entire spectrum of eigenvalues as a function of disorder. By increasing the disorder, the spectral gap closes, and generically, the IPRs increase, meaning that the states tend to localize on fewer and fewer sites. The smallest amount of disorder is enough to localize the entire spectrum. However, the $E = 0$ states, when facing disorder, become extended at some threshold values.

The left panel of Fig. 8 shows constant disorder cuts of the IPRs. For the clean system, the IPRs of the whole spectrum are $O(1/N)$, except for the MFs that live at $E = 0$. By adding disorder, they all become Anderson localized in the bulk. To understand the localization behavior of the Majorana zero modes, we pick four MFs (two pairs) and study their IPRs as a function of disorder. This is the content of the right panel of Fig. 8; blue and black symbols correspond to one pair of MFs, while red and green symbols correspond to the other pair. For small values of disorder, the IPRs for both pairs are a fraction of 1, which indicates extreme localization. By increasing disorder, the IPRs tend to decrease, meaning that MFs tend to become less localized. At the first threshold, the IPRs of the first pair reach a minimum, meaning that they are stretched as much as possible. At the first threshold value, the first pair of MFs whose IPRs have become small enough are drown into the bulk. This is signaled by the upturn in their IPRs. Such a monotonic increase in IPRs as a function of disorder is typical behavior of Anderson localized states. Therefore at the first threshold, the blue and black pair of MFs merges into the bulk of AL. The second pair (red and green curves) is, however, more resilient and refuses to delocalize further by approaching the first threshold. Beyond the first threshold W_{t1}, due to their Majorana character, their IPRs, unlike the Anderson localized states, decrease with increasing W. Finally, at the second threshold W_{t2} the resilience of the last pair of MFs is exhausted, and they surrender to disorder and merge into the bulk of Anderson localized states, which is signaled by the upturn in this curve. Beyond the second threshold, there are no more MF pairs left, and hence all the knots of the wave function are opened to give a zero-WN state. For disorder stronger than W_{t2} all states show a generic Anderson localization behavior of increasing IPRs as a function of the disorder.

The unusual (non-AL) decrease in IPRs of MFs gives them enough delocalization that allows them hybridize through higher-order processes within a nearly zero energy subspace of the Hilbert space. Increasing disorder enhances the density of nearly zero energy states, and hence there will be a large enough density of very low energy (localized) states that can mediate hybridization between the two Majorana partners at the two ends of the chain. In an empty lattice an IPR of $O(1/N)$ would be needed to qualify MFs for critical delocalization over the entire system. In the disordered case, although the minimum IPR is an order of magnitude larger than a fully extended state, the enhancement of the density of low-energy states (Fig. 4) allows them to efficiently hybridize and therefore unpins them from $E = 0$, ending their topological protection by saturating their resilience threshold. It is curious to note in the right panel of Fig. 8 that at the threshold values of disorder, not only do the *average* IPRs develop a minimum, but also the *fluctuations* of the IPRs are minimized. Understanding the fluctuations of IPRs for topological and nontopological states deserves a separate investigation [24].

So far we have found that the resilience threshold of Majorana fermions goes hand in hand with (i) a change in

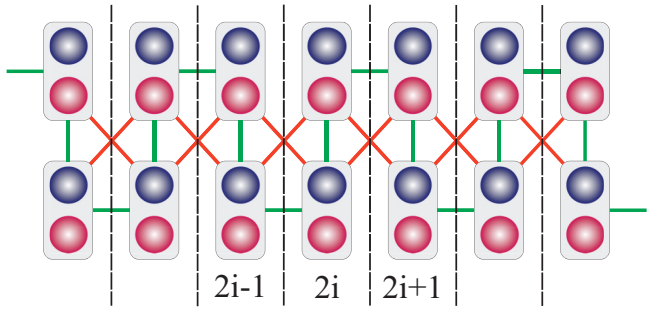

FIG. 9. Transfer matrix for our Hamiltonian. Each slice contains two atoms. Blue and red circles represent ψ^e and ψ^h, respectively. Green lines and orange lines show nearest- and next-nearest-neighbor couplings, respectively.

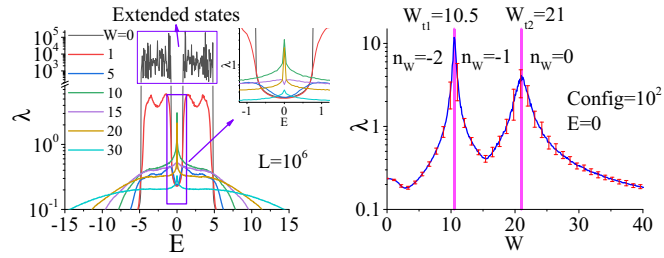

FIG. 10. Localization length versus energy for various W for the entire energy spectrum (left) and only $E = 0$ (i.e., MFs; right) as a function of disorder strength. The inset in the left panel indicates that for $W \approx 10$ and $W \approx 20$ the localization length diverges at $E = 0$. At topological transition points $W_{t1} = 10.5$ and $W_{t2} = 21$ the localization length of zero-energy states will diverge.

the absolute value of WN, which is accompanied by wild spatial fluctuations of the WN, (ii) a maximum in the density of zero-energy states as a function of disorder, (iii) minimal IPR fluctuations, and (iv) maximal extension of zero modes. The last fact allows us to use one of the powerful, precise, and fast techniques of Anderson localization physics, namely, the transfer-matrix (TM) method, not only as a way to determine the resilience threshold but also, by the above equivalence, as an alternative tool to diagnose the topological index of the system. This is the subject of the next section.

VI. RESILIENCE AND TRANSFER-MATRIX METHOD

So far we have identified the resilience threshold W_t of MFs in various quantities. The TM method, when appropriately modified to guarantee the convergence of the TM procedure, becomes a very cheap method to sharply determine W_t. This is the subject of the present section.

To calculate the localization length, we can use the quasi-one-dimensional Schrödinger equation $H\Psi_i = E\Psi_i$ [25,26]. In our model, we need to calculate the localization length for the wave functions in the Nambu space. When we have the next-nearest neighbor, we are led to organize the sites into the blocks depicted in Fig. 9 such that in the newly arranged form, the transfer of the amplitude of the wave function takes place only between neighboring blocks. In this basis, every block will have two sites, labeled by indices 1,2, and the wave function Ψ_i in the Nambu space will be $\Psi_i^T = (\psi^e_{i,1}, \psi^h_{i,1}, \psi^e_{i,2}, \psi^h_{i,2})$. This is effectively a four-channel quasi-one-dimensional problem. Within this representation, the wave equation becomes

$$t_{i,i-1}\Psi_{i-1} + H_{i,i}\Psi_i + t_{i,i+1}\Psi_{i+1} = E\Psi_i, \tag{21}$$

which can be rearranged to

$$\begin{pmatrix}\Psi_{i+1}\\ \Psi_i\end{pmatrix} = T_{i+1,i}\begin{pmatrix}\Psi_i\\ \Psi_{i-1}\end{pmatrix}, \tag{22}$$

where

$$T_{i+1,i} = \begin{pmatrix} t^{-1}_{i,i+1}(E - H_{i,i}) & -t^{-1}_{i,i+1}t_{i,i-1}\\ 1 & 0\end{pmatrix}. \tag{23}$$

As can be seen in Fig. 9, we have two types of slices, labeled $2i$ and $2i + 1$. The transfer matrix and on-site matrix for each slice are given by

$$t_{2i,2i+1} = t^T_{2i+1,2i} = \begin{pmatrix} 0 & 0 & J_2 & \lambda_2\\ 0 & 0 & -\lambda_2 & -J_2\\ J_2 & \lambda_2 & J_1 & \lambda_1\\ -\lambda_2 & -J_2 & -\lambda_1 & -J_1\end{pmatrix}, \tag{24a}$$

$$t_{2i+1,2i+2} = t^T_{2i+2,2i+1} = \begin{pmatrix} J_1 & \lambda_1 & J_2 & \lambda_2\\ -\lambda_1 & -J_1 & -\lambda_2 & -J_2\\ J_2 & \lambda_2 & 0 & 0\\ -\lambda_2 & -J_2 & 0 & 0\end{pmatrix}, \tag{24b}$$

$$H_{2i,2i} = \begin{pmatrix} \epsilon_{i,1} & 0 & J_1 & \lambda_1\\ 0 & -\epsilon_{i,1} & -\lambda_1 & -J_1\\ J_1 & -\lambda_1 & \epsilon_{i,2} & 0\\ \lambda_1 & -J_1 & 0 & -\epsilon_{i,2}\end{pmatrix}, \tag{24c}$$

$$H_{2i+1,2i+1} = \begin{pmatrix} \epsilon_{i,1} & 0 & J_1 & -\lambda_1\\ 0 & -\epsilon_{i,1} & \lambda_1 & -J_1\\ J_1 & \lambda_1 & \epsilon_{i,2} & 0\\ -\lambda_1 & -J_1 & 0 & -\epsilon_{i,2}\end{pmatrix}. \tag{24d}$$

To calculate the localization length at the end of the lattice, one needs to multiply the transfer matrices to form

$$\Gamma = \lim_{N\to\infty}\left[\prod_{i=N,1} T^{\dagger}_{i+1,i}\prod_{i=1,N} T_{i+1,i}\right]^{1/2N}. \tag{25}$$

Diagonalizing the above matrix gives $i = 1$–8 eigenvalues of the form $e^{\gamma_i L}$, where $L = N$ is the length of the system. Due to the symplectic form of the transfer matrix, the eigenvalues come in $e^{\pm\gamma L}$ pairs. The (largest) localization length λ is then calculated by

$$\lambda = \frac{1}{|\gamma_{\min}|}. \tag{26}$$

The details of obtaining the smallest positive Lyapunov exponent precisely can be found in Ref. [25,26]. In our calculation, we choose N large enough to guarantee the convergence of the localization length.

In the left panel of Fig. 10 we plot the localization length λ as a function of energy E of the states for various values of disorder W. For $W = 0$ all one-dimensional states, except

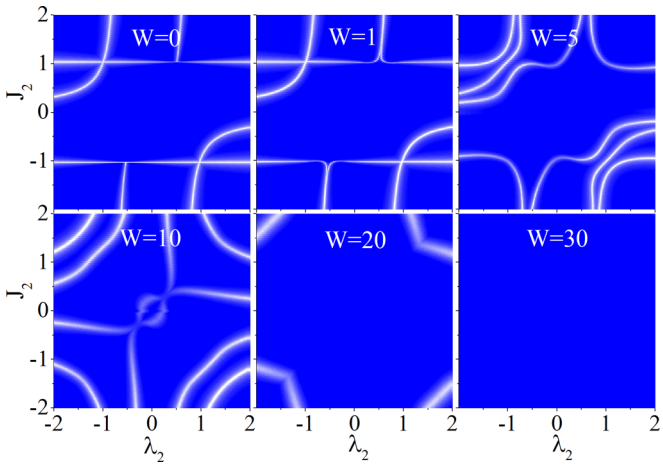

FIG. 11. Topological phase transitions from the localization length calculated by the transfer matrix. The localization length diverges at transition points.

the zero-energy Majorana modes, are extended. By adding the smallest amount of disorder, all bulk states become Anderson localized. By further increasing disorder (see the inset) the localization length at zero energy tends to develop a peak near the threshold values of $W \approx 10, 20$.

To see the critical delocalization of MFs at W_t, in the right panel of Fig. 10 we focus on the calculation of localization length for $E = 0$ Majorana modes. This shows a very clear indication of a divergence of the localization length of Majorana zero modes at the two threshold values indicated. The topological index (WN) is indicated. After each peak, the absolute value of the WN decreases by 1, and the system ultimately ends in a topologically trivial state with $n_w = 0$ at the strongest disorder regime. Viewing this sequence of one-by-one change in the WN in reverse elevates the TM method as a very quick method for the determination of n_w: The winding number can be determined by assigning zero to the most strongly disordered phase and increasing the absolute value by 1 upon crossing each divergence in λ of $E = 0$ Majorana modes. The sign of the winding number is a matter of convention and can be constructed from the symmetries of the Hamiltonian. Using the localization length λ of Majorana zero modes to map the phase diagram of the disordered 2XY model, we can sharply determine the phase boundaries. The phase boundaries are given in Fig. 11. Figure 11 agrees with Fig. 6, but Fig. 11 is more accurate, and moreover in Fig. 11, it is much easier to determine phase boundaries with the transfer-matrix method. Without knowledge of Fig. 6 the WN can be assigned to Fig. 11 up to an overall sign ambiguity, as explained above.

The localization length as calculated from the Lyapunov exponent in the TM method provides not only a very precise but also numerically very economic (as it requires the TM procedure for only $E = 0$ energy) determination of the resilience threshold of Majorana zero modes which also coincides with the onset of the change in the WN. The divergence of localization length at the resilience threshold furthermore identifies the threshold of resilience with the maximal stretchability of MFs and hence substantiates the claim of critical delocalization of MFs at the threshold values. Since the transfer-matrix method is essentially free from finite-size errors, as the amplitude of the wave function can be transferred up to arbitrarily long distances, the system at the threshold values of the disorder must be scale invariant. This entitles the disorder-induced topological phase transitions to some sort of order parameter which can be encoded into an appropriate nonlinear-σ model in supersymmetry approaches [1].

Note that the diverging length scale is a peculiar feature of MF zero modes. All other states are Anderson localized for the smallest disorder and therefore are left with no sense of the length scale of the entire system.

VII. CONCLUSION

We investigated the mechanism of change in the WN by the disorder in an extension of the Kitaev chain, dubbed the 2XY model [12]. Possible realizations of longer-range hopping can be achieved by an array of magnetic nanoparticles placed on a superconductor [27]. We established that every pair of MFs has a threshold resilience at which they critically delocalize and hence hybridize and unpin from $E = 0$. This is how they lose their topological protection and become part of the Anderson localized bulk states. This explains why, in the presence of disorder, across every boundary the WN changes by only 1. After corroborating with costly and established methods of calculation of the topological index based on the polarization, we showed that the above resilience threshold can easily and precisely be determined by simply looking at the divergence of the localization length of *only* the $E = 0$ states (corresponding to MFs). We curiously observed that at the threshold values, not only do the IPRs of $E = 0$ states reach a minimum, but the *fluctuations* of the IPRs are also suppressed. We furthermore showed that the resilience threshold is precisely where the WN changes by 1. Given this, the localization length can be employed to sharply determine the winding number in the BDI class of topological insulators. Note that this method makes no reference to the polarization (related to the Berry phase).

It is desirable to incorporate the above observations to construct an effective order parameter theory to address the interplay between the p-wave superconductivity and disorder [28]. The analogy with plateau-to-plateau transitions in the quantum Hall effect and possible effective theories with the θ term [29] or possible renormalization group interpretation [30] is worth exploring.

ACKNOWLEDGMENTS

We acknowledge discussions with A. Nersesyan and M. Dalmonte of the Abdus Salam ICTP.

APPENDIX A: KERNEL POLYNOMIAL METHOD

In the kernel polynomial method [19–22] one expands the spectral functions in a set of orthonormal polynomials. The coefficients of expansion will be appropriate matrix elements or traces. Then the traces can be stochastically calculated. Consider a Hamiltonian H with energy eigenvalues E in the range $[E_{\min}, E_{\max}]$. To expand in Chebyshev polynomials, which are defined for arguments whose magnitude does not exceed 1, one should first rescale the Hamiltonian from

$H(E)$ to $\hat{H}(\varepsilon)$, where $\hat{H} = (H - b)/a$, $\varepsilon = (E - b)/a$, $b = (E_{\max} + E_{\min})/2$, and $a = (E_{\max} - E_{\min})/2$. The normalized density of states can be expanded for the range $\varepsilon \in [-1, 1]$ into Chebyshev polynomials as

$$\hat{\rho}(\varepsilon) = \frac{1}{\pi\sqrt{1-\varepsilon^2}}\left(\mu_0 g_0 + 2\sum_{m=1}^{N_c}\mu_m g_m T_m(\varepsilon)\right), \quad \text{(A1)}$$

where $T_m(\varepsilon) = \cos[m \arccos(\varepsilon)]$ are the mth Chebyshev polynomials, μ_m are Chebyshev moments, and g_m are the so-called attenuation factors to minimize the Gibbs oscillations. N_c is a cutoff on the order of polynomials used in the expansion. μ_m is given by a trace formula, $\mu_m = 1/M \sum_{r=1}^{M}\langle\phi_r|T_m(\hat{H})|\phi_r\rangle$. Since the trace does not depend on the basis, we can choose ϕ_r as random single-particle states, and we should use M as the number of random states used in the evaluation of the trace. To obtain matrix elements of $T_m(\hat{H})$ we can use the recurrence relation of Chebyshev polynomials, $T_m(\hat{H}) = 2\hat{H}T_{m-1}(\hat{H}) - T_{m-2}(\hat{H})$ with initial conditions $T_1(\hat{H}) = \hat{H}$ and $T_0(\hat{H}) = 1$. This enables the computation of spectral functions without explicit diagonalization of the Hamiltonian.

APPENDIX B: WINDING NUMBER

This Appendix is based entirely on the work of Proden and colleagues [18,23]. The idea is to homotopically deform a given Hamiltonian H to its flat band equivalent given by

$$H \to Q = P_+ - P_-, \quad \text{(B1)}$$

where P_- and P_+ are projection operators of filled and empty bands, respectively, and are given by

$$P_+ = \sum_{E_n > E_f}|n\rangle\langle n|, \quad P_- = 1 - P_+. \quad \text{(B2)}$$

Since in our model the chiral symmetry operator satisfies $S = S^\dagger$ and $S^2 = 1$, the eigenvalues of S are ± 1. Defining $S_\pm$ as the projection operator to the space of these eigenvalues, it can be represented as $S = S_+ - S_-$. Every chiral symmetric operator, including Q, can be represented as $Q = S_+QS_- + S_-QS_+$, where $(S_\pm QS_\mp)^\dagger = S_\mp QS_\pm$ and $(S_\pm QS_\mp)^{-1} = S_\mp QS_\pm$. Then the WN can be calculated from the above canonical form using $Q_{+-} = S_+QS_-$, $(Q_{+-})^{-1} = S_-QS_+ = Q_{-+}$. Replacing ∂_k with $-i[X, \cdot]$, where X is the position operator, and denoting the summation over k space degrees of freedom (per volume) by tr, the WN in real space is given by

$$n_w = -\mathrm{tr}\{Q_{-+}[X, Q_{+-}]\}. \quad \text{(B3)}$$

For a given realization of disorder, this formula allows the calculation of the WN in a single diagonalization procedure. Further averaging over disorder smoothens the variations of the above WN.

[1] A. Altland, D. Bagrets, and A. Kamenev, Phys. Rev. B **91**, 085429 (2015).
[2] J. Li, R.-L. Chu, J. K. Jain, and S.-Q. Shen, Phys. Rev. Lett. **102**, 136806 (2009).
[3] Y. Hatsugai, K. Ishibashi, and Y. Morita, Phys. Rev. Lett. **83**, 2246 (1999).
[4] J. Song and E. Prodan, Phys. Rev. B **92**, 195119 (2015).
[5] R. Bianco and R. Resta, Phys. Rev. B **84**, 241106 (2011).
[6] Z. F. Zhang, Y. Y. Yang, Y. Ju, L. Sheng, R. Shen, D. N. Sheng, and D. Y. Xing, Chin. Phys. B **22**, 117312 (2013).
[7] R. Ghadimi, T. Sugimoto, and T. Tohyama, J. Phys. Soc. Jpn. **86**, 114707 (2017).
[8] E. V. Castro, M. P. López-Sancho, and M. A. H. Vozmediano, Phys. Rev. B **92**, 085410 (2015).
[9] A. Altland and M. R. Zirnbauer, Phys. Rev. B **55**, 1142 (1997).
[10] C.-K. Chiu, J. C. Teo, A. P. Schnyder, and S. Ryu, Rev. Mod. Phys. **88**, 035005 (2016).
[11] M. Greiter, V. Schnells, and R. Thomale, Ann. Phys. (NY) **351**, 1026 (2014).
[12] S. A. Jafari and F. Shahbazi, Sci. Rep. **6**, 32720 (2016).
[13] W. DeGottardi, M. Thakurathi, S. Vishveshwara, and D. Sen, Phys. Rev. B **88**, 165111 (2013).
[14] S. Vishveshwara and M. P. A. Fisher, Phys. Rev. B **64**, 174511 (2001).
[15] A. Y. Kitaev, Phys. Usp. **44**, 131 (2001).
[16] I. Mahyaeh and E. Ardonne, J. Phys. Commun. **2**, 045010 (2018).
[17] S. Lieu, D. K. Lee, and J. Knolle, arXiv:1804.10908.
[18] E. Prodan and H. Schulz-Baldes, J. Funct. Anal. **271**, 1150 (2016).
[19] H. Lee, J. Kim, E. R. Mucciolo, G. Bouzerar, and S. Kettemann, Phys. Rev. B **85**, 075420 (2012).
[20] M. Amini, S. A. Jafari, and F. Shahbazi, Europhys. Lett. **87**, 37002 (2009).
[21] A. Habibi and S. A. Jafari, J. Phys.: Condens. Matter **25**, 375501 (2013).
[22] A. Weiße, G. Wellein, A. Alvermann, and H. Fehske, Rev. Mod. Phys. **78**, 275 (2006).
[23] I. Mondragon-Shem, T. L. Hughes, J. Song, and E. Prodan, Phys. Rev. Lett. **113**, 046802 (2014).
[24] F. Evers and A. D. Mirlin, Phys. Rev. Lett. **84**, 3690 (2000).
[25] A. MacKinnon and B. Kramer, Phys. Rev. Lett. **47**, 1546 (1981).
[26] A. MacKinnon and B. Kramer, Z. Phys. B **53**, 1 (1983).
[27] T.-P. Choy, J. M. Edge, A. R. Akhmerov, and C. W. J. Beenakker, Phys. Rev. B **84**, 195442 (2011).
[28] R. Sknepnek, T. Vojta, and R. Narayanan, Phys. Rev. B **70**, 104514 (2004).
[29] A. Pruisken, Int. J. Theor. Phys. **48**, 1736 (2009).
[30] S. A. Jafari, Phys. Rev. E **96**, 012159 (2017).